HOKKAIDO UNIVERSITY

Title	Wiener-Based Inpainting Quality Prediction
Author(s)	OGAWA, Takahiro; TANAKA, Akira; HASEYAMA, Miki
Citation	IEICE Transactions on Information and Systems, E100.D(10), 2614-2626 https://doi.org/10.1587/transinf.2017EDP7058
Issue Date	2017-10-01
Doc URL	http://hdl.handle.net/2115/67806
Rights	Copyright © 2017 The Institute of Electronics, Information and Communication Engineers
Type	article
File Information	Wiener-Based Inpainting Quality Prediction.pdf

PAPER
Wiener-Based Inpainting Quality Prediction*

Takahiro OGAWA[†a)], Akira TANAKA[†], *and* Miki HASEYAMA[†], *Members*

SUMMARY A Wiener-based inpainting quality prediction method is presented in this paper. The proposed method is the first method that can predict inpainting quality both before and after the intensities have become missing even if their inpainting methods are unknown. Thus, when the target image does not include any missing areas, the proposed method estimates the importance of intensities for all pixels, and then we can know which areas should not be removed. Interestingly, since this measure can be also derived in the same manner for its corrupted image already including missing areas, the expected difficulty in reconstruction of these missing pixels is predicted, i.e., we can know which missing areas can be successfully reconstructed. The proposed method focuses on expected errors derived from the Wiener filter, which enables least-squares reconstruction, to predict the inpainting quality. The greatest advantage of the proposed method is that the same inpainting quality prediction scheme can be used in the above two different situations, and their results have common trends. Experimental results show that the inpainting quality predicted by the proposed method can be successfully used as a universal quality measure.

key words: *quality prediction, inpainting, Wiener filter, least-squares estimation*

1. Introduction

Inpainting has various fundamental applications such as unnecessary object removal [1]–[5] and error concealment [6]–[9]. It is important to predict inpainting quality for a target image both before and after its intensities have become missing. Specifically, if a measure representing inpainting quality is estimated for all of the pixels within an original image, we can know which areas within the target image must not be removed. Furthermore, if this measure is calculated for a corrupted image including missing areas, the difficulty in reconstruction of the missing pixels, i.e., expected errors caused in the missing intensity estimation, can be predicted. The difficulty in reconstruction of missing areas should ideally be predicted in the same manner for both of the above different situations.

Inpainting quality can be predicted by monitoring simple statistics such as variances in small regions within a target image. However, accurate prediction becomes difficult for regions including high-frequency components such as textures. The simplest approach is to apply an existing in-painting and image completion method to artificially added missing areas and use their errors observed from the reconstruction results. Unfortunately, this approach cannot be applied to the situation after intensities have been removed from target images. Furthermore, this approach cannot provide expected errors without performing the reconstruction procedure.

Prediction of inpainting quality is closely related to the problem of estimating the importance of pixels within a target image, e.g., saliency estimation. Many methods for computing saliency of a target image have been proposed. Koch and Ullman carried out a pioneering work in which a computational model of visual attention was constructed for the first time [10]. Based on this model, Itti et al. proposed a bottom-up approach for generating saliency maps that can provide salient regions within target images [11]. This method became one of the representative methods in the research field of saliency estimation. This method has also been improved by many researchers. Harel et al. proposed a graph-based implementation of the Itti and Koch model, Graph-Based Visual Saliency (GBVS), and achieved improvement in performance [12]. An approach that focuses on the Fourier domain has also been proposed for saliency estimation. Hou et al. proposed a method that included a spectral residual approach [13]. In recent studies, a Discrete Cosine Transform (DCT)-based method, image signature, has been used for highlighting sparse salient regions [14]. Several methods with approaches that are different from those of the above-described methods have also been proposed. Bruce et al. proposed a new model for saliency computation based on an information theoretic formulation dubbed Attention based on Information Maximization (AIM) [15]. In addition, Gofeman et al. proposed detection of "image regions that represent the scene", which are different from the most salient regions [16]. Navalpakkam et al. proposed a Signal-to-Noise Ratio (SNR)-based saliency that represents the ratio of expected salience of the target over distractors [17]–[19]. The above-described existing methods are only a few of the many attractive methods, and good survey reports in this research field have been published by several researchers [20]–[22].

It should be noted that although the above-described approaches can reveal which areas are important within target images, it is difficult to predict the difficulty in reconstruction of missing areas within corrupted images. Therefore, a new measure is necessary for realizing the above goal. Some researchers have proposed inpainting quality

assessment methods that focus on evaluating the inpainting performance [23], [24]. However, the target of this method is quality assessment of inpainting results, and it evaluates how successfully the missing areas can be recovered. Therefore, this method cannot predict inpainting quality for both original images and their corrupted images including missing areas.

In this paper, we present a Wiener-based inpainting quality prediction method. In terms of least-squares reconstruction, the Wiener filter [25] is the best and most fundamental method since it is well known that its criterion is for minimizing the expected mean square error (MSE). This means that the Wiener filter is an ideal reconstruction method minimizing the expected MSE. Therefore, the proposed method focuses on the expected MSE derived in the Wiener filter to predict the reconstruction difficulty, this measure hereafter being denoted as Wiener-based inpainting quality. In the proposed method, this measure can be derived from both an original image and its corrupted image including missing areas in the same manner. Specifically, when the target image does not include any missing areas, the proposed method can predict which areas should not be missed since the importance of all of pixels is estimated. On the other hand, when some intensities are missing within the target image, the proposed method can predict which missing areas can be successfully reconstructed since the difficulty in reconstruction of the missing pixels is estimated. In these two situations, "the importance of the known original pixels" and "the difficulty in reconstruction of missing pixels" can be commonly derived by the proposed method. To the best of our knowledge, our method is the first method that realizes prediction of inpainting quality that can be derived in the two different situations. Interestingly, the results of prediction in these two different situations have the same trends.

There are several applications of the proposed method such as improvement in image coding efficiency and error concealment. For example, in the field of image coding, improvement in coding efficiency can be achieved by artificially adding missing blocks to a target image in an encoder side and recovering them in a decoder side [3], [26]–[28]. Our method enables determination of the optimal positions of blocks that have been removed, which can be successfully recovered in the decoder side. Furthermore, in error concealment, since a packet loss causes missing blocks, these blocks must be recovered or their correct packets must be retransmitted for maintaining high image quality [6]–[9]. Therefore, for determining the optimal choice, our method is necessary to predict image quality after the reconstruction of missing blocks.

2. Wiener Filter

In this section, a brief explanation of the Wiener filter [25] used in the proposed method is given. Reconstruction of corrupted images based on the Wiener filter is shown in 2.1, and error analysis of the Wiener filter is shown in 2.2.

2.1 Image Reconstruction Based on the Wiener Filter

Given a corrupted image including some degradations, we focus on reconstruction of its original image based on the Wiener filter. First, we denote all original patches within a target image as f_i ($i \in \mathcal{I}; \mathcal{I} = \{1, 2, \cdots, N\}$). Furthermore, we denote patches including some degradations, e.g., missing areas, blurring, etc., as g_j ($j \in \mathcal{J}$; $\mathcal{J} \subset \mathcal{I}$) within its corrupted image. Next, we define two vectors $\mathbf{x}_i$ ($i \in \mathcal{I}$) and $\mathbf{y}_j$ ($j \in \mathcal{J}$) whose elements are intensities in the original patches f_i and intensities in the corrupted patches g_j, respectively. The relationship between f_j and g_j ($j \in \mathcal{J}$) is written as follows:

$$\mathbf{y}_j = \mathbf{M}_j \mathbf{x}_j + \mathbf{n} \quad (j \in \mathcal{J}), \tag{1}$$

where $\mathbf{M}_j$ is a matrix that represents the degradation of g_j, and $\mathbf{n}$ represents a noise vector that is independent of the original vector $\mathbf{x}_j$. Since we focus on missing area reconstruction in the following section, we can ignore this noise vector hereafter. Given two correlation matrices $\mathbf{R_x}$ and $\hat{\mathbf{R}}_\mathbf{x}$ as

$$\mathbf{R_x} = \frac{1}{|\mathcal{J}|} \sum_{j \in \mathcal{J}} \mathbf{x}_j \mathbf{x}_j', \tag{2}$$

$$\hat{\mathbf{R}}_\mathbf{x} = \frac{1}{|\mathcal{I} - \mathcal{J}|} \sum_{k \in \mathcal{I} - \mathcal{J}} \mathbf{x}_k \mathbf{x}_k' \tag{3}$$

for $\mathbf{x}_j$ ($j \in \mathcal{J}$) and $\mathbf{x}_k$ ($k \in \mathcal{I} - \mathcal{J}$), respectively, the ideal reconstruction result $\mathbf{x}_j^W$ from $\mathbf{y}_j$ based on the Wiener filter is obtained as follows:

$$\mathbf{x}_j^W = \mathbf{R_x} \mathbf{M}_j' \left(\mathbf{M}_j \mathbf{R_x} \mathbf{M}_j' \right)^+ \mathbf{y}_j, \tag{4}$$

where $(\cdot)^+$ represents the calculation of a pseudo inverse matrix. Furthermore, $|\cdot|$ in Eqs. (2) and (3) represents the number of elements that belong to a target set. Furthermore, vector/matrix transpose is denoted as a superscript $'$ in this paper. Unfortunately, since g_j ($j \in \mathcal{J}$) are corrupted, the correlation matrix $\mathbf{R_x}$ in Eq. (2) is unknown when calculating Eq. (4). Therefore, in many cases, $\hat{\mathbf{R}}_\mathbf{x}$ in Eq. (3) is adopted instead of $\mathbf{R_x}$ to obtain the following result:

$$\mathbf{x}_j^{W*} = \hat{\mathbf{R}}_\mathbf{x} \mathbf{M}_j' \left(\mathbf{M}_j \hat{\mathbf{R}}_\mathbf{x} \mathbf{M}_j' \right)^+ \mathbf{y}_j. \tag{5}$$

Then reconstruction of the corrupted patches g_j ($j \in \mathcal{J}$) based on the Wiener filter becomes feasible.

2.2 Error Analysis of the Wiener Filter

Given a corrupted patch g whose corresponding original vector and degradation matrix are denoted as $\mathbf{x}$ and $\mathbf{M}$, respectively, the mean of the expected squared errors of the estimation result $\mathbf{x}^{W*}$ based on Eq. (5) from the corrupted vector of $\mathbf{x}$ is derived as follows:

$$e^W = \frac{E_\mathbf{x} \left\{ \left\| \mathbf{x} - \mathbf{x}^{W*} \right\|^2 \right\}}{d}$$
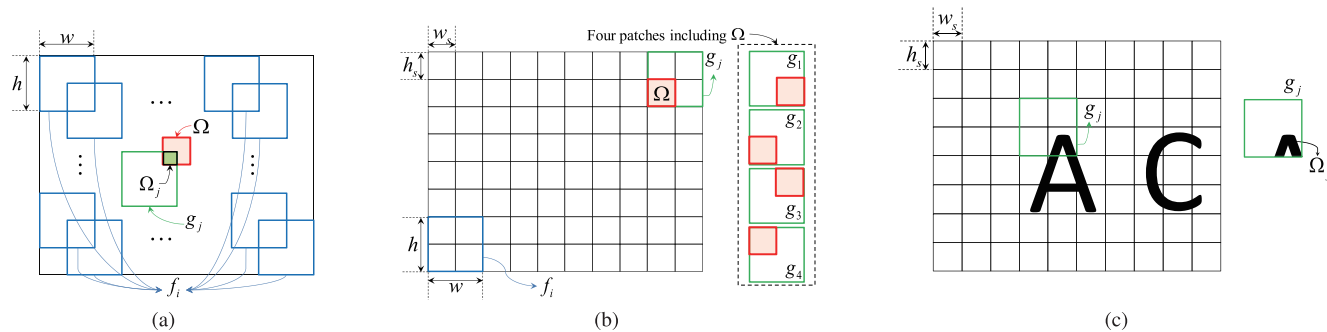
Fig. 1 (a) Relationships between f_i ($i \in \mathcal{I}$), g_j ($j \in \mathcal{J}$), Ω and Ω_j, (b) estimation of e_Ω^W for a target area Ω based on Eq. (24), where e_Ω^W is calculated from four patches including Ω in this example, (c) estimation of $\hat{e}_j^W$ of a missing area Ω_j in patch g_j ("A" and "C" corresponding to missing areas Ω).

$$= \frac{tr\,[\mathbf{S}\mathbf{R}_\mathbf{x}\mathbf{S}']}{d}, \tag{6}$$

where $E_\mathbf{x}\{\cdot\}$ is an operator calculating an expectation value of $\cdot$ in terms of a random vector $\mathbf{x}$, $\mathbf{x}^{W*}$ can be obtained in the same manner as Eq. (5), $tr(\cdot)$ calculates a trace of a target matrix, d is the dimension of $\mathbf{x}$, and

$$\mathbf{S} = \mathbf{I}_d - \hat{\mathbf{R}}_\mathbf{x}\mathbf{M}'\left(\mathbf{M}\hat{\mathbf{R}}_\mathbf{x}\mathbf{M}'\right)^+ \mathbf{M}. \tag{7}$$

In the above equation, $\mathbf{I}_d$ is the $d \times d$ identity matrix.

It should be noted that if the degradation is intensity removal, $\mathbf{M}$ becomes a diagonal matrix whose diagonal elements are one or zero. Then, by focusing only on reconstruction of the missing area of g, e^W can be rewritten as

$$\begin{aligned} e^W &= \frac{E_\mathbf{x}\left\{\left\|(\mathbf{I}_d - \mathbf{M})\left(\mathbf{x} - \mathbf{x}^{W*}\right)\right\|^2\right\}}{tr\,(\mathbf{I}_d - \mathbf{M})} \\ &= \frac{tr\,[(\mathbf{I}_d - \mathbf{M})\,\mathbf{S}\mathbf{R}_\mathbf{x}\mathbf{S}'\,(\mathbf{I}_d - \mathbf{M})]}{tr\,(\mathbf{I}_d - \mathbf{M})}. \end{aligned} \tag{8}$$

Before intensities within an area have become missing, we can calculate the expected errors as shown in the above equation. However, after the intensities have become missing, we cannot obtain $\mathbf{R}_\mathbf{x}$ in Eq. (8), and we therefore use $\hat{\mathbf{R}}_\mathbf{x}$ instead of $\mathbf{R}_\mathbf{x}$ and can obtain the following alternative expected error:

$$\hat{e}^W = \frac{tr\left[(\mathbf{I}_d - \mathbf{M})\,\mathbf{S}\hat{\mathbf{R}}_\mathbf{x}\mathbf{S}'\,(\mathbf{I}_d - \mathbf{M})\right]}{tr\,(\mathbf{I}_d - \mathbf{M})}. \tag{9}$$

This means that we assume the correlation matrix $\hat{\mathbf{R}}_\mathbf{x}$ is the same as $\mathbf{R}_\mathbf{x}$. If the target corrupted patch can be easily complemented by the other known parts within the target image, this assumption tends to be satisfied.

3. Wiener-Based Inpainting Quality Prediction

In this section, the method for predicting Wiener-based inpainting quality is presented. First, in 3.1, we show the derivation of inpainting quality for images not including missing areas and generation of an inpainting quality map. Next, in 3.2, derivation of inpainting quality for corrupted images including missing areas and generation of the corresponding inpainting quality map are described.

3.1 Inpainting Quality Prediction for Images Not Including Missing Areas

First, we denote a local area (a local block) in which the inpainting quality is predicted within the target image as Ω. In this subsection, we derive inpainting quality representing the importance of the target area Ω in terms of the Wiener filter-based expected error. First, we denote a set of indices as $\mathcal{I} = \{1, 2, \cdots, N\}$ and define a set of d-dimensional vectors obtained from patches f_i ($i \in \mathcal{I}$; $w \times h = d$ pixels) within the target image $\mathcal{X} = \left\{\mathbf{x}_i \in \mathbf{R}^d | i \in \mathcal{I}\right\}$. Furthermore, patches g_j ($j \in \mathcal{J} \subset \mathcal{I}$) include the target area Ω, and $\mathbf{y}_j$ are defined as vectors of patches g_j ($j \in \mathcal{J}$), whose intensities included within Ω are removed from $\mathbf{x}_j$. Thus, the following relationship is satisfied:

$$\mathbf{y}_j = \mathbf{M}_j\mathbf{x}_j \quad (j \in \mathcal{J}), \tag{10}$$

where $\mathbf{M}_j \in \mathbf{R}^{d \times d}$ is a diagonal matrix, whose diagonal elements are one or zero, for removing intensities within Ω. Figure 1 (a) shows an example of the relationship between the patches f_i ($i \in \mathcal{I}$), g_j ($j \in \mathcal{J}$) and the target area Ω. As shown in this figure, we denote the overlapped area included in both Ω and g_j ($j \in \mathcal{J}$) as Ω_j.

In terms of the Wiener filter-based expected error, we first try to predict the inpainting quality of area Ω_j included in g_j ($j \in \mathcal{J}$). First, assuming that $\text{rank}\left(\mathbf{M}_j\right) = r_j < d$, we define $\mathbf{P}_j \in \mathbf{R}^{r_j \times d}$ obtained by removing zero row vectors from $\mathbf{M}_j$. Furthermore, $\mathbf{Q}_j \in \mathbf{R}^{(d-r_j) \times d}$ is obtained by removing rows included in $\mathbf{P}_j$ from the identity matrix $\mathbf{I}_d \in \mathbf{R}^{d \times d}$. Then, by calculating $\mathbf{P}_j\mathbf{x}_j$, only the known intensities within $\mathbf{y}_j$ can be extracted. On the other hand, by calculating $\mathbf{Q}_j\mathbf{x}_j$, only the missing intensities removed from $\mathbf{x}_j$ can be extracted. Therefore, from the above definitions,

$$\mathbf{P}_j'\mathbf{P}_j + \mathbf{Q}_j'\mathbf{Q}_j = \mathbf{I}_d \tag{11}$$

and

$$\mathbf{Q}_j\mathbf{P}_j' = \mathbf{O}_{(d-r_j) \times r_j} \tag{12}$$

are satisfied, where $\mathbf{O}_{(d-r_j) \times r_j}$ is the $(d-r_j) \times r_j$ zero matrix.

Next, as a problem for estimating $\mathbf{x}_j$ from $\mathbf{y}_j$, we try to estimate the following matrix $\mathbf{W}_j$:

$$\mathbf{W}_j = \arg \min_{\mathbf{W}} J(\mathbf{W}), \tag{13}$$

where

$$J(\mathbf{W}) = E_{\mathbf{x}_j} \left[\left\| \mathbf{W} \mathbf{P}_j \mathbf{y}_j - \mathbf{Q}_j \mathbf{x}_j \right\|^2 \right]. \tag{14}$$

Note that

$$\mathbf{P}_j \mathbf{y}_j = \mathbf{P}_j \mathbf{x}_j \tag{15}$$

is satisfied, and by regarding $\mathbf{x}_j$ as a random vector $\mathbf{x}$, Eq. (14) is rewritten as

$$\begin{aligned}
J(\mathbf{W}) &= E_{\mathbf{x}_j} \left[\left\| \mathbf{W} \mathbf{P}_j \mathbf{x}_j - \mathbf{Q}_j \mathbf{x}_j \right\|^2 \right] \\
&= E_{\mathbf{x}} \left[\left\| \mathbf{W} \mathbf{P}_j \mathbf{x} - \mathbf{Q}_j \mathbf{x} \right\|^2 \right] \\
&= E_{\mathbf{x}} \left[tr \left\{ \left(\mathbf{W} \mathbf{P}_j - \mathbf{Q}_j \right) \mathbf{x} \mathbf{x}' \left(\mathbf{W} \mathbf{P}_j - \mathbf{Q}_j \right)' \right\} \right] \\
&= tr \left[\left(\mathbf{W} \mathbf{P}_j - \mathbf{Q}_j \right) E_{\mathbf{x}} \left\{ \mathbf{x} \mathbf{x}' \right\} \left(\mathbf{W} \mathbf{P}_j - \mathbf{Q}_j \right)' \right] \\
&= tr \left[\left(\mathbf{W} \mathbf{P}_j - \mathbf{Q}_j \right) \mathbf{R}_{\mathbf{x}} \left(\mathbf{W} \mathbf{P}_j - \mathbf{Q}_j \right)' \right], \tag{16}
\end{aligned}$$

where $\mathbf{R}_{\mathbf{x}} \in \mathcal{R}^{d \times d}$ is a correlation matrix of $\mathbf{x}$ and should be defined as follows:

$$\mathbf{R}_{\mathbf{x}} = \frac{1}{|\mathcal{J}|} \sum_{j \in \mathcal{J}} \mathbf{x}_j \mathbf{x}_j', \tag{17}$$

where $|\mathcal{J}|$ is the number of elements belonging to $\mathcal{J}$. However, when estimating intensities within Ω_j, $\mathbf{R}_{\mathbf{x}}$ is unknown. Thus, it must be approximately estimated from $\mathbf{x}_k$ ($k \in \mathcal{I} - \mathcal{J}$) as follows:

$$\hat{\mathbf{R}}_{\mathbf{x}} = \frac{1}{|\mathcal{I} - \mathcal{J}|} \sum_{k \in \mathcal{I} - \mathcal{J}} \mathbf{x}_k \mathbf{x}_k', \tag{18}$$

where $|\mathcal{I} - \mathcal{J}|$ is the number of elements belonging to $\mathcal{I} - \mathcal{J}$. Then Eq. (16) is rewritten as

$$J(\mathbf{W}) = tr \left[\left(\mathbf{W} \mathbf{P}_j - \mathbf{Q}_j \right) \hat{\mathbf{R}}_{\mathbf{x}} \left(\mathbf{W} \mathbf{P}_j - \mathbf{Q}_j \right)' \right]. \tag{19}$$

Based on the derivation shown in the previous section, the solution of Eq. (13) can be obtained as follows:

$$\mathbf{W}_j = \mathbf{Q}_j \hat{\mathbf{R}}_{\mathbf{x}} \mathbf{P}_j' \left(\mathbf{P}_j \hat{\mathbf{R}}_{\mathbf{x}} \mathbf{P}_j' \right)^+. \tag{20}$$

Therefore, the estimation result of the intensities included in Ω_j within $\mathbf{y}_j$ is obtained as

$$\mathbf{z}_j = \mathbf{W}_j \mathbf{P}_j \mathbf{y}_j. \tag{21}$$

In the proposed method, we have to predict the inpainting quality of the area Ω_j in terms of the Wiener filter-based expected error. This means that we try to estimate the expected error caused in the recovery of the area Ω_j when its intensities are missing. Thus, for each g_j ($j \in \mathcal{J}$), the mean of the expected errors in Ω_j can be obtained as

$$\begin{aligned}
e_j^W &= E_{\mathbf{x}_j} \left[\frac{\left\| \mathbf{z}_j - \mathbf{Q}_j \mathbf{x}_j \right\|^2}{\text{rank}(\mathbf{Q}_j)} \right] \\
&= E_{\mathbf{x}_j} \left[\frac{\left\| \mathbf{W}_j \mathbf{P}_j \mathbf{y}_j - \mathbf{Q}_j \mathbf{x}_j \right\|^2}{\text{rank}(\mathbf{Q}_j)} \right] \\
&= E_{\mathbf{x}_j} \left[\frac{\left\| \mathbf{W}_j \mathbf{P}_j \mathbf{x}_j - \mathbf{Q}_j \mathbf{x}_j \right\|^2}{\text{rank}(\mathbf{Q}_j)} \right] \\
&= E_{\mathbf{x}_j} \left[\frac{\left\| \left(\mathbf{W}_j \mathbf{P}_j - \mathbf{Q}_j \right) \mathbf{x}_j \right\|^2}{\text{rank}(\mathbf{Q}_j)} \right], \tag{22}
\end{aligned}$$

where the third equivalence holds since Eq. (15) is satisfied. Furthermore, by regarding $\mathbf{x}_j$ as a random vector $\mathbf{x}$, the above equation can be rewritten as follows:

$$\begin{aligned}
e_j^W &= E_{\mathbf{x}} \left[\frac{\left\| \left(\mathbf{W}_j \mathbf{P}_j - \mathbf{Q}_j \right) \mathbf{x} \right\|^2}{\text{rank}(\mathbf{Q}_j)} \right] \\
&= \frac{E_{\mathbf{x}} \left[tr \left\{ \left(\mathbf{W}_j \mathbf{P}_j - \mathbf{Q}_j \right) \mathbf{x} \mathbf{x}' \left(\mathbf{W}_j \mathbf{P}_j - \mathbf{Q}_j \right)' \right\} \right]}{\text{rank}(\mathbf{Q}_j)} \\
&= \frac{tr \left[\left(\mathbf{W}_j \mathbf{P}_j - \mathbf{Q}_j \right) E_{\mathbf{x}} \left\{ \mathbf{x} \mathbf{x}' \right\} \left(\mathbf{W}_j \mathbf{P}_j - \mathbf{Q}_j \right)' \right]}{\text{rank}(\mathbf{Q}_j)} \\
&= \frac{tr \left[\left(\mathbf{W}_j \mathbf{P}_j - \mathbf{Q}_j \right) \mathbf{R}_{\mathbf{x}} \left(\mathbf{W}_j \mathbf{P}_j - \mathbf{Q}_j \right)' \right]}{\text{rank}(\mathbf{Q}_j)}. \tag{23}
\end{aligned}$$

Then the Wiener-based inpainting quality of the target area Ω is obtained as follows:

$$e_\Omega^W = \frac{1}{|\mathcal{J}|} \sum_{j \in \mathcal{J}} e_j^W. \tag{24}$$

This equation calculates the mean of e_j^W for all Ω_j ($j \in \mathcal{J}$) within Ω. In this way, prediction of the inpainting quality of intensities within the target area Ω becomes feasible.

Finally, we explain the method for calculating an inpainting quality map for an image that does not include any missing areas. The inpainting quality map represents the importance of each pixel within the target image. In the proposed method, we divide the target image into small blocks ($w_s \times h_s$ pixels; $w_s < w$ and $h_s < h$), and each small block is regarded as Ω as shown in Fig. 1 (b). Furthermore, the horizontal and vertical clipping intervals of patches f_i ($i \in \mathcal{I}$) and g_j ($j \in \mathcal{J}$) are w_s and h_s pixels, respectively. Then the importance of each area Ω can be calculated as e_Ω^W by using Eq. (24). If the importance of the area Ω is higher, the value of e_Ω^W also becomes higher since its reconstruction becomes difficult when its intensities are missing. Therefore, by calculating e_Ω^W for all of the small areas with a size of $w_s \times h_s$ pixels, an inpainting quality map of the target image can be obtained.

Table 1 The comparative methods used in this experiment and their notations. In this table, we also show the MSE of the reconstruction results (Wiener, BPLP and Exemplar) obtained for the image shown in Fig. 2.

Methods	Ref. [11]	Ref. [12]	Ref. [13]	Ref. [15]	Ref. [14]	Ref. [16]	Proposed method
Notations	Itti98	GBVS07	SR07	AIM09	SIG12	CAS12	Ours
MSE of Wiener	4.07×10	1.23×10^2	2.23×10	6.25×10	3.05×10	4.87×10	$\mathbf{1.01 \times 10}$
MSE of BPLP	1.64×10^2	4.27×10^2	8.19×10	2.31×10^2	1.42×10^2	3.16×10^2	$\mathbf{2.39 \times 10}$
MSE of Exemplar	1.16×10^2	2.76×10^2	6.32×10	1.36×10^2	1.11×10^2	1.35×10^2	$\mathbf{3.60 \times 10}$

3.2 Inpainting Quality Prediction for Corrupted Images Including Missing Areas

In this subsection, we show inpainting quality prediction for a corrupted image including missing areas. Given a corrupted image including missing areas Ω, the inpainting quality of the sub-missing area Ω_j is calculated for each corrupted patch g_j $(j \in \mathcal{J})$ as shown in Fig. 1 (c). Note that Ω represents all of the missing areas within the target image, and the definitions of f_i $(i \in \mathcal{I})$, g_j $(j \in \mathcal{J})$ and Ω_j are the same as those shown in the previous subsection. Then the quality measure can be derived in the same manner as Eq. (23). Note that in Eq. (23), the correlation matrix $\mathbf{R_x}$ is unknown. Thus, we introduce one assumption: $\mathbf{R_x} = \hat{\mathbf{R}}_\mathbf{x}$. Then the estimate of Eq. (23) is obtained as follows:

$$\hat{e}_j^W = \frac{tr\left[\left(\mathbf{W}_j\mathbf{P}_j - \mathbf{Q}_j\right)\hat{\mathbf{R}}_\mathbf{x}\left(\mathbf{W}_j\mathbf{P}_j - \mathbf{Q}_j\right)'\right]}{\text{rank}\left(\mathbf{Q}_j\right)}. \quad (25)$$

If the target image uniformly has similar statistical features in all parts, the assumption $\mathbf{R_x} = \hat{\mathbf{R}}_\mathbf{x}$ tends to be satisfied. Then $\hat{e}_j^W$ in Eq. (25) can accurately approximate e_j^W in Eq. (23). Therefore, the proposed method can derive the inpainting quality in the same manner before and after the intensities within the target image have become missing.

Next, we explain the method for calculating the inpainting quality map, which is calculated for the missing areas and represents their expected reconstruction difficulty. In the proposed method, we clip the patches f_i $(i \in \mathcal{I})$ and g_j $(j \in \mathcal{J})$ in the same intervals, the horizontal and vertical intervals being w_s and h_s pixels, respectively ($w_s < w$ and $h_s < h$), as shown in Fig. 1 (c). Then, for each patch g_j, its expected error $\hat{e}_j^W$ caused in the missing area Ω_j is calculated. Since the clipped patches g_j are overlapped blocks, multiple results are obtained for each pixel within the missing areas. Therefore, by averaging these multiple results for each missing pixel, we can obtain the inpainting quality map.

4. Experimental Results

In order to verify the performance of the proposed method, experimental results obtained by applying the Wiener-based inpainting quality prediction method and other existing methods to several test images are shown in this section. The inpainting quality obtained by the proposed method can be utilized as two measures, importance of known original pixels and expected difficulty in reconstruction of missing areas. Therefore, we first show verification of the performance of the former measure, i.e., calculation of the importance of known original pixels, of our method by comparing with other existing methods in Sect. 4.1. Next, in 4.2, we show verification of the performance of the latter measure by applying our inpainting quality prediction method to several corrupted images including missing areas. Therefore, the experimental results presented in 4.1 and 4.2 correspond to the methods shown in 3.1 and 3.2, respectively.

It should be noted that in the experiments, we used missing square blocks since our target applications are improvement in image coding efficiency and error concealment as shown in Sect. 1. Furthermore, our method is the first trial that can predict the inpainting quality in the same manner before and after intensities have become missing. Therefore, it is most important to verify the fundamental performance of the quality prediction based on experiments focusing on our target applications.

4.1 Performance Verification of Inpainting Quality Prediction for Images Not Including Missing Areas

This subsection shows the performance verification of our inpainting quality prediction for images not including missing areas. In this experiment, we picked up pixels as missing regions based on our prediction method, inpainted them, and calculated MSE against the original input image with the inpainted image. Then we try to show that if the MSEs of several inpainting methods are small, our proposed prediction method can choose pixels to be easily inpainted by all of the inpainting methods and vise versa.

In this experiment, we used 120 benchmark test images that were published by Bruce et al. [15][†]. Inpainting quality maps for these test images were calculated by using the proposed method. Inpainting quality maps were also generated by using other existing methods shown in Table 1. The first column of Fig. 2 shows an example of the inpainting quality maps obtained by our method and the existing methods[††]. From the top row to the bottom row, we show the results of Itti98, GBVS07, SR07, AIM09, SIG12, CAS12 and Ours shown in Table 1, respectively. It should be noted that since a method for predicting inpainting quality before intensities become missing has not been proposed, we performed the

---

[†]http://www-sop.inria.fr/members/Neil.Bruce/

[††]In this experiment, we directly used the source codes published by the authors of the comparative methods, and their conditions were based on their published papers.

Fig. 2 Results obtained by using the comparative methods and the proposed method. From the top row to the bottom row, we show the results of Itti98, GBVS07, SR07, AIM09, SIG12, CAS12 and Ours shown in Table 1, respectively.

comparison with saliency estimation methods, which are approaches that are the most similar to ours. Therefore, we used the saliency maps obtained by these methods as inpainting quality maps.

The first, second, third and fourth columns of Fig. 2 show inpainting quality maps, corrupted images including

missing areas for which positions were determined according to these maps, results of reconstruction by using the Wiener filter [25] and results of reconstruction by using the
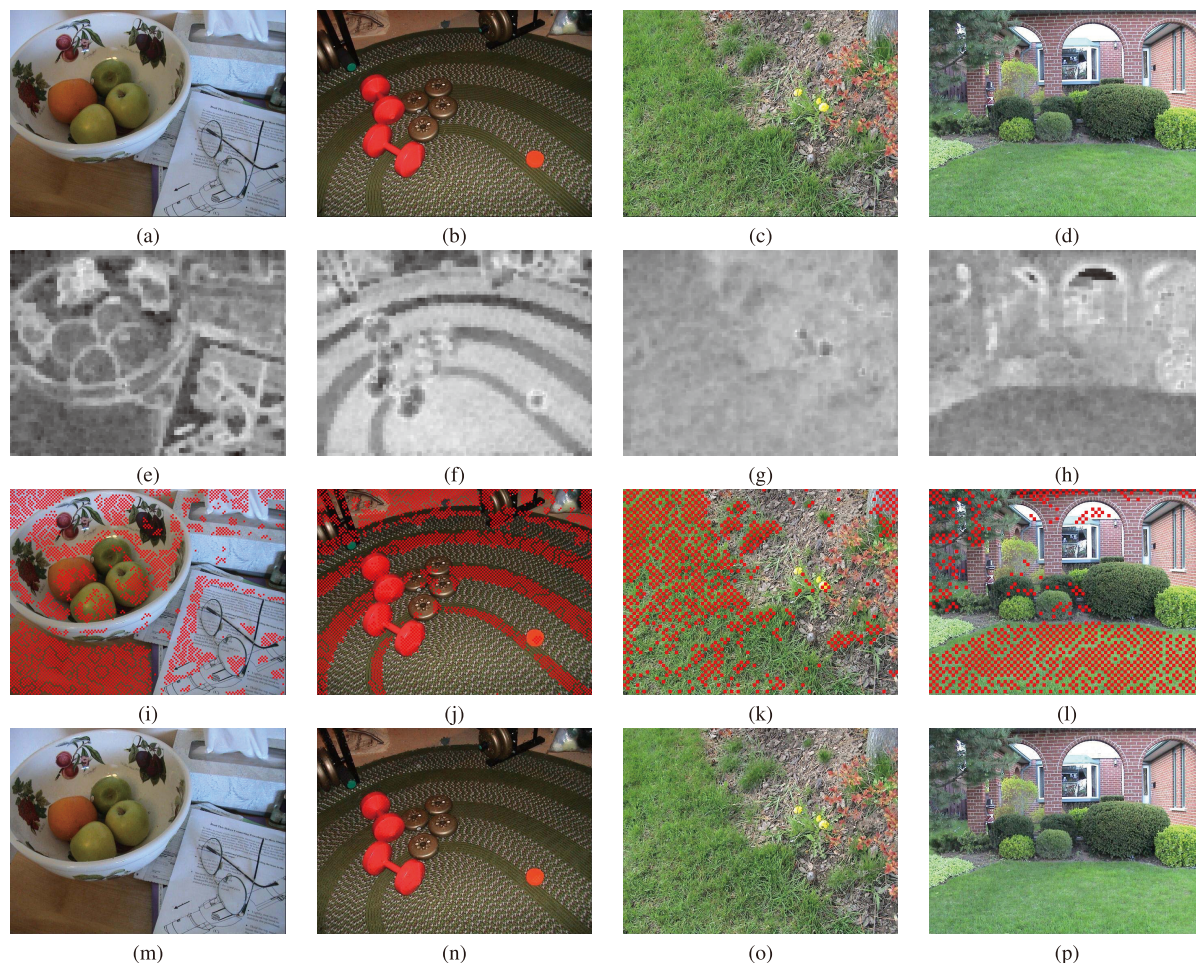
Fig. 3 Examples of inpainting quality maps obtained by using the proposed method and the reconstruction results of missing blocks added according to the obtained inpainting quality maps: (a)–(d) original images, (e)–(h) inpainting quality maps of (a)–(d) obtained by the proposed inpainting quality prediction method, (i)–(l) images including missing blocks added according to the inpainting quality maps in (e)–(h), and (m)–(p) reconstruction results of (i)–(l) by the Wiener filter. The missing block sizes are 4×4 pixels in (i) and (j) and 8×8 pixels in (k) and (l). The percentage of missing pixels is 16% for all examples.

exemplar-based method [4], respectively[†]. In this figure, the size of missing blocks is 4×4 pixels, and the percentage of missing pixels is 12%. In the proposed method, we set $w = h = 8$ and $w_s = h_s = 4$. From the obtained results, the inpainting quality maps generated by our method and other existing methods are different, but it is difficult to know which methods can generate an optimal map that correctly represents the importance of each area. Therefore, in this experiment, we performed evaluation based on the following schemes.
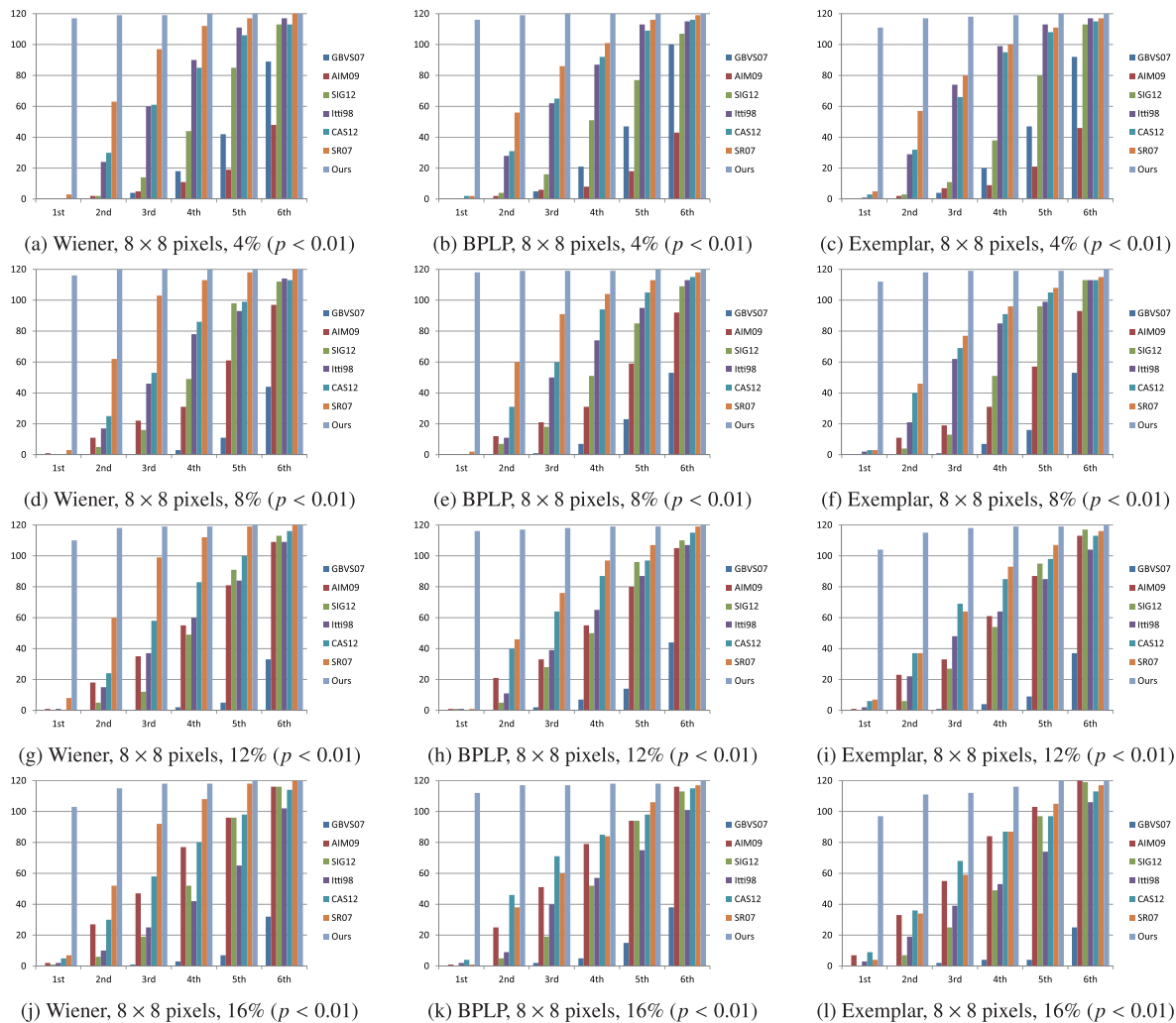
First, we added missing blocks to the original images

as low-priority blocks according to the inpainting quality maps. Specifically, we iteratively removed the intensities of the blocks in which the sum of inpainting quality values was the smallest. If missing blocks existed in four neighboring blocks, we did not remove the target blocks for the following reconstruction procedures. The results obtained from inpainting quality maps generated by our method and other existing methods in the first column of Fig. 2 are shown in the second column of this figure. For those images, we performed reconstruction of the missing areas by using three previously reported benchmarking methods: Wiener filter [25], BPLP (Back Projection for Lost Pixels) method [5] and an exemplar-based method [4]. The BPLP method [5] is different from the Wiener filter, but it is closely related to the correlation matrix focused on in the proposed method.

The reconstruction results obtained by two methods (Wiener filter and exemplar-based method) are shown in the third and fourth columns of Fig. 2, respectively. Due

---

[†]We published supplemental materials showing the high-resolution version of Figs. 2 and 3 in the following URL: https://www-lmd.ist.hokudai.ac.jp/member/takahiro-ogawa/wiqp/ In these supplemental materials, the images are shown in their original resolution. From the results, we can see that the proposed method tends to be able to successfully remove and recover regions which are simple and can be easily estimated from the other remaining regions.
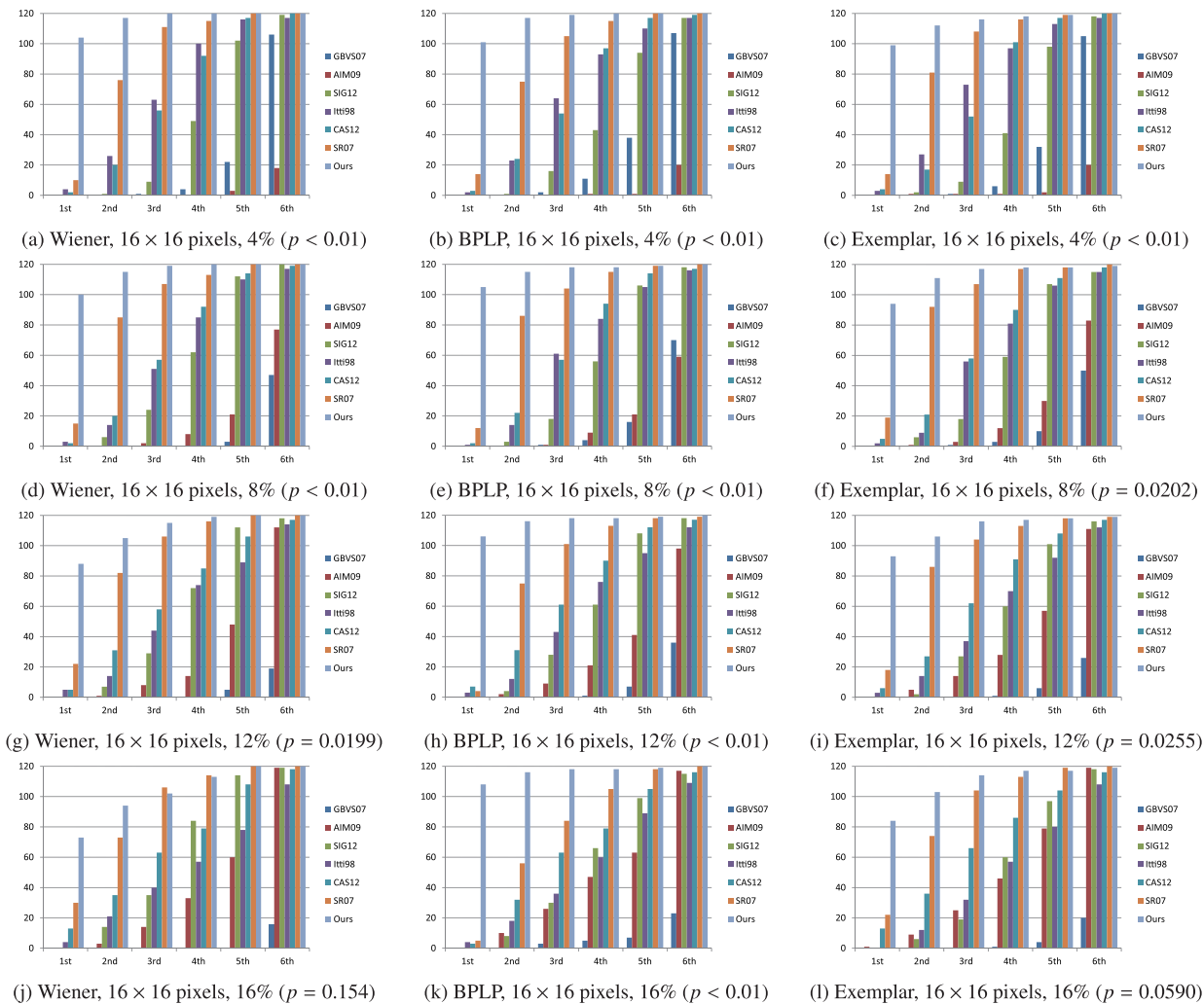
Fig. 4 Results of ranking obtained for different reconstruction methods (Wiener, BPLP and Exemplar) and different percentages of missing pixels (4%, 8%, 12% and 16%). This figure shows the results obtained by using missing blocks with sizes of 8×8 pixels. The text in each caption includes the reconstruction method, missing block size, percentage of missing pixels and results of the statistical test. The value of the nth rank represents the number of images included up to the nth rank in each method, i.e., the number of images included in 1st, 2nd, $\cdots$, nth ranks.

to limitation of space, only results obtained by using these two methods are shown in this figure. Table 1 shows the MSEs of the reconstruction results for quantitatively evaluating the obtained results. The MSE obtained from the proposed method is smaller than those of other existing methods.

We also show some other examples obtained by the proposed method. Figure 3 shows results obtained in the same manner as that for the results shown in Fig. 2. From the four images shown in Figs. 3 (a)–(d), we calculated their inpainting quality maps as shown in Figs. 3 (e)–(h). According to the obtained maps, missing blocks were added to these test images as shown in Figs. 3 (i)–(l). For these corrupted images including missing blocks, we performed reconstruction by using the Wiener filter as shown in Figs. 3 (m)–(p). The results showed that successful reconstruction is feasible and also indicated that areas that should not be removed

can be successfully found by the inpainting quality maps obtained by our method.

Next, in order to quantitatively evaluate the performance of the proposed method, we show other results obtained from the 120 test images. We added missing blocks (8×8 pixels and 16×16 pixels) to these 120 test images with changes in the percentage of missing pixels (4%, 8%, 12% and 16%) according to the inpainting quality maps obtained by our method and other comparative methods. Then the corrupted test images were recovered by using the Wiener filter, the BPLP method and the exemplar-based method. For each test image, we performed ranking of our method and other comparative methods according to MSE calculated from the reconstruction results as shown in Table 1. The first rank corresponds to the method for which MSE is lowest, and the lowest rank corresponds to the method for which MSE is highest.

(a) Wiener, 16×16 pixels, 4% ($p < 0.01$)

(b) BPLP, 16×16 pixels, 4% ($p < 0.01$)

(c) Exemplar, 16×16 pixels, 4% ($p < 0.01$)

(d) Wiener, 16×16 pixels, 8% ($p < 0.01$)

(e) BPLP, 16×16 pixels, 8% ($p < 0.01$)

(f) Exemplar, 16×16 pixels, 8% ($p = 0.0202$)

(g) Wiener, 16×16 pixels, 12% ($p = 0.0199$)

(h) BPLP, 16×16 pixels, 12% ($p < 0.01$)

(i) Exemplar, 16×16 pixels, 12% ($p = 0.0255$)

(j) Wiener, 16×16 pixels, 16% ($p = 0.154$)

(k) BPLP, 16×16 pixels, 16% ($p < 0.01$)

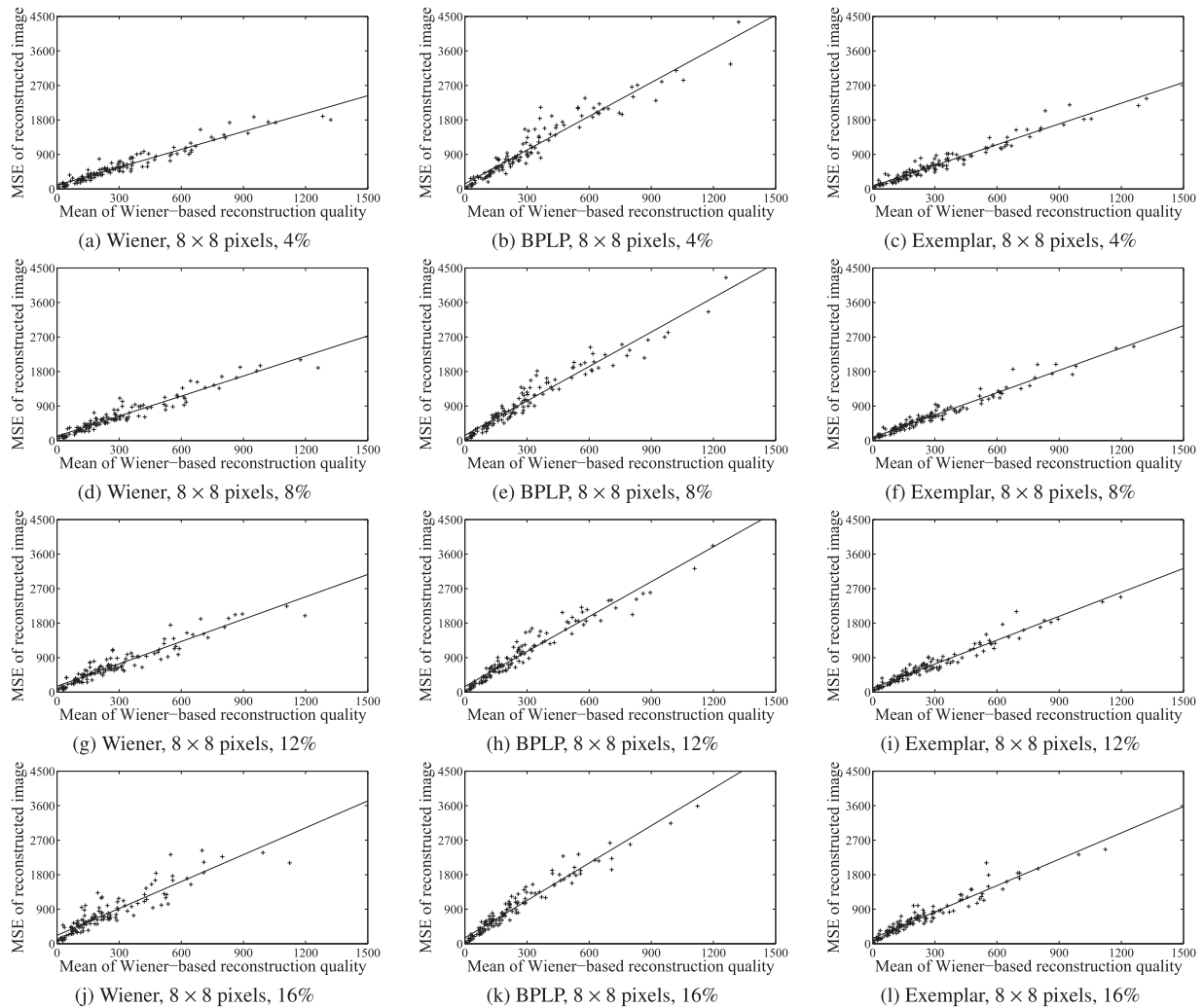(l) Exemplar, 16×16 pixels, 16% ($p = 0.0590$)

Fig. 5 Results of ranking obtained for different reconstruction methods (Wiener, BPLP and Exemplar) and different percentages of missing pixels (4%, 8%, 12% and 16%). This figure shows the results obtained by using missing blocks with sizes of 16×16 pixels. The text in each caption is the same as that shown in Fig. 4.

Figures 4 and 5 show the results of the ranking obtained for the different reconstruction methods (Wiener, BPLP and Exemplar), different missing block sizes (8×8 pixels and 16×16 pixels) and different percentages of missing pixels (4%, 8%, 12% and 16%). In these figures, the value of the nth rank in each method represents the number of images that are included up to the nth rank, i.e., the number of images included in 1st, 2nd, $\cdots$, nth ranks. From Fig. 4, it can be seen that for almost all test images, the proposed method achieves the first rank when using the Wiener filter and the BPLP method. Even when the exemplar-based method was used, the proposed method gave much better results than the results of comparative methods. The results obtained by the Wiener filter are quite natural since we used Wiener-based inpainting quality. On the other hand, the BPLP method and the exemplar-based method also gave better results when using the proposed inpainting quality prediction method. Figure 5 shows the results for missing blocks with sizes of

16×16 pixels. As shown in this figure, the proposed method also outperforms the comparative methods for all patterns. The results shown in these figures indicate that the proposed method is optimal for estimating which areas should not be missed.

In order to justify the superiority of the proposed method, we also performed a statistical test. Figures 4 and 5 show the ranking of the MSE calculated from the images reconstructed by the Wiener filter, the BPLP method and the exemplar-based method. We performed Welch's t-test to confirm the significance of the difference between the MSE of the proposed method and those of the conventional methods. We assumed the null hypothesis "The mean value of MSE obtained from the 120 images by our method and that obtained by the comparative method are equal", where the significance level was set as $\alpha = 0.01$. From the results obtained by this statistical test (p-values shown in Figs. 4 and 5), the superiority of our method can be almost confirmed.

(a) Wiener, 8×8 pixels, 4%

(b) BPLP, 8×8 pixels, 4%

(c) Exemplar, 8×8 pixels, 4%

(d) Wiener, 8×8 pixels, 8%

(e) BPLP, 8×8 pixels, 8%

(f) Exemplar, 8×8 pixels, 8%

(g) Wiener, 8×8 pixels, 12%

(h) BPLP, 8×8 pixels, 12%

(i) Exemplar, 8×8 pixels, 12%

(j) Wiener, 8×8 pixels, 16%

(k) BPLP, 8×8 pixels, 16%

(l) Exemplar, 8×8 pixels, 16%

Fig. 6 Relationship between mean of Wiener-based inpainting quality and MSE of the reconstructed image when using missing blocks with sizes of 8×8 pixels. The text in each caption includes the reconstruction method, missing block size and percentage of missing pixels. The dots shown in each graph represent results for 120 images, and the line is the regression line obtained from the 120 samples. The horizontal and vertical axes are the mean value calculated from the proposed inpainting quality map and MSE calculated between the reconstructed image by Wiener, BPLP and Exemplar and its original image, respectively.

Table 2 Subjective evaluation results (average and standard deviation of rating scores). Given a significance level $\alpha = 0.01$, it was confirmed that our method is superior to the other comparative methods by Welch's t-test with $p < 0.01$.

Methods	Itti98	GBVS07	SR07	AIM09	SIG12	CAS12	Ours
Scores	2.96 ± 1.26	2.22 ± 0.893	3.25 ± 1.24	3.69 ± 0.934	2.74 ± 0.989	2.50 ± 1.25	$\mathbf{4.04 \pm 1.08}$

Note that p-values were obtained between our method and the next best method.

Next, we show results of subjective testing. In this experiment, we randomly selected 20 images from the 120 images and performed the same experiments to obtain reconstruction results by the Wiener filter that correspond to the third column of Fig. 2, where the percentage of removed pixels was set to 16% for enhancing the difference between the seven methods shown in Table 1. The size of missing blocks was randomly selected from 4×4 pixels, 8×8 pix-

els or 16×16 pixels. Seventeen subjects participated in this experiment, and each subject performed rating for the reconstruction results with rating scores ranging from 1 (bad) to 5 (good). Since 20 test images were used, each subject rated 140 (20×7) images totally. The results of the subjective evaluation are shown in Table 2. From the obtained results, we can see that the average score of the proposed method is higher than those of the other comparative methods. Furthermore, we found that our method was statistically superior to the other comparative methods by Welch's t-test as
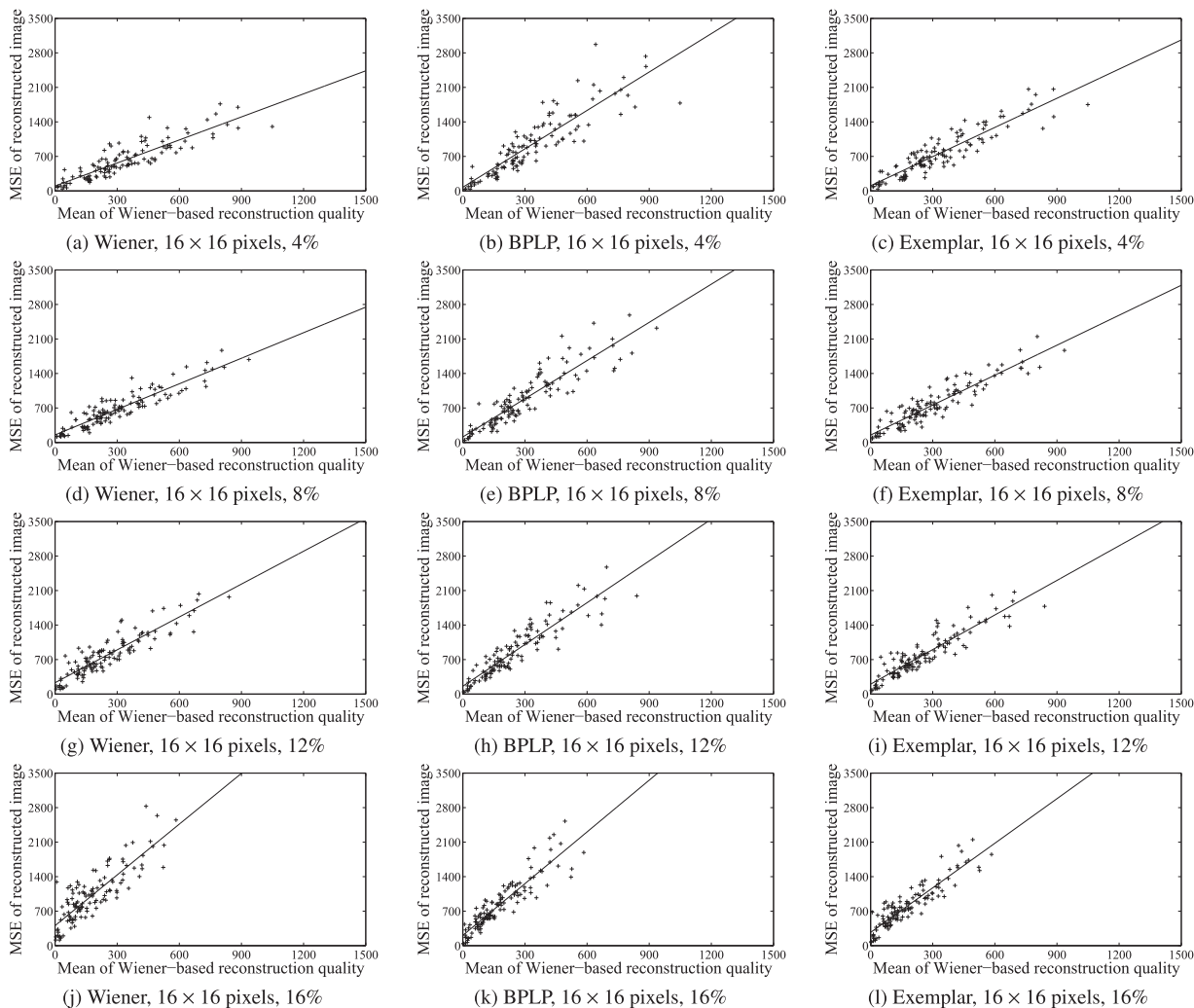
Fig. 7 Relationship between mean of Wiener-based inpainting quality and the MSE of the reconstructed image when using missing blocks with sizes of 16×16 pixels. The details of this figure are the same as those in Fig. 6.

shown in the caption of Table 2. Therefore, the effectiveness of the proposed inpainting quality prediction was also confirmed in this experiment.

4.2 Performance Verification of Inpainting Quality Prediction for Corrupted Images Including Missing Areas

In this subsection, we show verification of the performance of expected reconstruction difficulty predicted for missing areas by using the proposed method. We performed the inpainting quality prediction for missing areas within given images, inpainted them, and calculated MSE against their original images with the inpainted images. Then we try to show that if the correlation between the inpainting quality prediction results and MSEs of every inpainting methods is high, our method can find whether the target images including missing areas can be easily inpainted or not by all of the inpainting methods and vise versa.

In this experiment, we used the same 120 test images

shown in the previous subsection. We randomly added missing blocks with sizes of 8×8 pixels and 16×16 pixels to these test images. The missing block size corresponds to $w_s \times h_s$ pixels, and the patch size ($w \times h$ pixels) was set to twice its size. For these corrupted images, we calculated the inpainting quality map, i.e., the reconstruction difficulty map shown in 3.2.

From the corrupted images, we performed reconstruction of the missing areas by using the Wiener filter, the BPLP method and the exemplar-based method. Figures 6 and 7 show the relationship between the mean of Wiener-based inpainting quality and MSE of the reconstructed image. Note that the mean of Wiener-based inpainting quality can be obtained by calculating the mean of the inpainting quality map. The line shown in each graph is the regression line obtained from the 120 samples, i.e., the 120 test images.

From the results shown in these figures, we can see predicted quality by the proposed method and MSE of the reconstruction results have a strong correlation. Pearson and

Table 3 Correlation coefficients (Pearson correlation) between mean of Wiener-based reconstruction difficulty and MSE of the recovered image by each reconstruction method.

Block size	Percentage	Wiener	BPLP	Exemplar
8×8 pixels	4%	0.964	0.960	0.972
8×8 pixels	8%	0.961	0.969	0.979
8×8 pixels	12%	0.947	0.970	0.975
8×8 pixels	16%	0.912	0.972	0.963
16×16 pixels	4%	0.881	0.888	0.913
16×16 pixels	8%	0.917	0.908	0.920
16×16 pixels	12%	0.901	0.917	0.912
16×16 pixels	16%	0.846	0.913	0.910

Table 4 Correlation coefficients (Spearman correlation) between mean of Wiener-based reconstruction difficulty and MSE of the recovered image by each reconstruction method.

Block size	Percentage	Wiener	BPLP	Exemplar
8×8 pixels	4%	0.961	0.970	0.962
8×8 pixels	8%	0.956	0.976	0.972
8×8 pixels	12%	0.940	0.973	0.969
8×8 pixels	16%	0.920	0.975	0.961
16×16 pixels	4%	0.892	0.921	0.901
16×16 pixels	8%	0.903	0.923	0.598
16×16 pixels	12%	0.883	0.931	0.897
16×16 pixels	16%	0.806	0.930	0.888

Spearman correlation coefficients calculated from the results in Figs. 6 and 7 are shown in Tables 3 and 4, respectively. The correlation coefficients are very high for all of the reconstruction methods.

5. Conclusions

In this paper, we have proposed Wiener-based inpainting quality prediction for missing intensity estimation. Since the expected errors caused in the reconstruction can be derived by using the Wiener filter, the proposed method defines the inpainting quality from the derived expected errors. Then the importance of each pixel, i.e., which areas should not be missed, can be estimated from the target image. Furthermore, by calculating our novel measure for its corrupted image including missing areas, the expected difficulty in reconstruction of these missing areas can be also predicted. In the experiments, it was verified that the proposed method has good performance for prediction of inpainting quality, and it would be useful in several applications.

Finally, we show limitations and future directions of our method. As shown in 3.2, we assume that $\mathbf{R_x} = \hat{\mathbf{R}}_{\mathbf{x}}$ to derive Eq. (25). However, if this assumption is not satisfied in a given image, it becomes difficult to successfully estimate Eq. (25), and this phenomenon will be significant when missing areas Ω become larger. Furthermore, there are some regions in which the proposed method fails to estimate the corrupted image, e.g., edges of the picture hanged on the wall in Fig. 2. We guess that since the inpainting quality prediction model shown in the proposed method is closely related to the positions of missing pixels from its definition but does not consider structure components of target images, the proposed method incorrectly selects regions including edges. Therefore, it may be useful in our method to collaborate with some visual saliency estimation methods.

In this study, we derived the inpainting quality by using MSE. However, in several studies on image quality assessment [29], [30], it has been shown that several different measures can reflect human perceptual qualities more successfully than MSE-based measures. Therefore, by replacing MSE with such better quality measures, perceptually optimized inapinting quality prediction will become feasible.

References

[1] C. Ballester, M. Bertalmio, V. Caselles, G. Sapiro, and J. Verdera, "Filling-in by joint interpolation of vector fields and gray levels," IEEE Transactions on Image Processing, vol.10, no.8, pp.1200–1211, 2001.

[2] A. Kokaram, "A statistical framework for picture reconstruction using 2D AR models," Image and Vision Computing, vol.22, no.2, pp.165–171, 2004.

[3] S.D. Rane, G. Sapiro, and M. Bertalmio, "Structure and texture filling-in of missing image blocks in wireless transmission and compression applications," IEEE Transactions on Image Processing, vol.12, no.3, pp.296–303, 2003.

[4] A. Criminisi, P. Perez, and K. Toyama, "Region filling and object removal by exemplar-based image inpainting," IEEE Transactions on Image Processing, vol.13, no.9, pp.1200–1212, 2004.

[5] T. Amano and Y. Sato, "Image interpolation using BPLP method on the eigenspace," Systems and Computers in Japan, vol.38, no.1, pp.87–96, 2007.

[6] W.-Y. Kung, C.-S. Kim, and C.-C.J. Kuo, "Spatial and temporal error concealment techniques for video transmission over noisy channels," IEEE Transactions on Circuits and Systems for Video Technology, vol.16, no.7, pp.789–803, 2006.

[7] M. Ma, O.C. Au, S.-H.G. Chan, and M.-T. Sun, "Edge-directed error concealment," IEEE Transactions on Circuits and Systems for Video Technology, vol.20, no.3, pp.382–395, 2010.

[8] Y. Zhang, X. Xiang, D. Zhao, S. Ma, and W. Gao, "Packet video error concealment with auto regression model," IEEE Transactions on Circuits and Systems for Video Technology, vol.22, no.1, pp.12–27, 2012.

[9] Z. Cui, Z. Gan, X. Zhan, and X. Zhu, "Error concealment techniques for video transmission over error-prone channels: A Survey," Journal of Computational Information Systems, vol.8, no.21, pp.8807–8818, 2012.

[10] C. Koch and S. Ullman, "Shifts in selective visual attention: towards the underlying neural circuitry," Human Neurobiology, vol.4, no.4, pp.219–227, 1985.

[11] L. Itti, C. Koch, and E. Niebur, "A model of saliency-based visual attention for rapid scene analysis," IEEE Transactions on Pattern Analysis and Machine Intelligence, vol.20, no.11, pp.1254–1259, 1998.

[12] J. Harel, C. Koch, and P. Perona, "Graph-based visual saliency," Advances in Neural Information Processing Systems 19, MIT Press, pp.545–552, 2007.

[13] X. Hou and L. Zhang, "Saliency detection: A spectral residual approach," Proc. IEEE Computer Society Conference on Computer Vision and Pattern Recognition (CVPR), pp.1–8, 2007.

[14] X. Hou, J. Harel, and C. Koch, "Image signature: Highlighting sparse salient regions," IEEE Transactions on Pattern Analysis and Machine Intelligence, vol.34, no.1, pp.194–201, 2012.

[15] N.D.B. Bruce and J.K. Tsotsos, "Saliency, attention, and visual search: An information theoretic approach," Journal of Vision, vol.9, no.3, pp.1–24, 2009.

[16] S. Goferman, L. Zelnik-Manor, and A. Tal, "Context aware saliency detection," IEEE Transactions on Pattern Analysis and Machine Intelligence, vol.34, no.10, pp.1915–1926, 2012.

[17] V. Navalpakkam and L. Itti, "An integrated model of top-down and bottom-up attention for optimizing detection speed," Proc. IEEE Computer Society Conference on Computer Vision and Pattern Recognition (CVPR), vol.2, pp.2049–2056, 2006.

[18] V. Navalpakkam and L. Itti, "Modeling the influence of task on attention," Vision Research, vol.45, no.2, pp.205–231, 2005.

[19] V. Navalpakkam and L. Itti, "Search goal tunes visual features optimally," Neuron, vol.53, pp.605–617, 2007.

[20] S. Frintrop, E. Rome, and H.I. Christensen, "Computational visual attention systems and their cognitive foundations: A survey," ACM Transactions on Applied Perception, vol.7, no.1, pp.6:1–6:39, 2010.

[21] A.L. Rothenstein and J.K. Tsotsos, "Attention links sensing to recognition," Image and Vision Computing, vol.26, no.1, pp.114–126, 2008.

[22] J. Tilke, F. Durand, and A. Torralba, "A Benchmark of Computational Models of Saliency to Predict Human Fixations," MIT Computer Science and Artificial Intelligence Laboratory Technical Report, 2012.
Available online: http://dspace.mit.edu/handle/1721.1/68590

[23] P.A. Ardis, C.M. Brown, and A. Singhal, "Inpainting quality assessment," Journal of Electronic Imaging, vol.19, no.1, 2010.

[24] M. Isogawa, D. Mikami, K. Takahashi, and A. Kojima, "Eye gaze analysis and learning-to-rank to obtain the most preferred result in image inpainting," Proc. 2016 IEEE International Conference on Image Processing (ICIP), pp.3538–3542, 2016.

[25] H. Ogawa and E. Oja, "Projection filter, Wiener filter, and Karhunen-Loève subspaces in digital image restoration," Journal of Mathematical Analysis and Applications, vol.114, no.1, pp.37–51, 1986.

[26] D. Liu, X. Sun, F. Wu, S. Li, and Y.-Q. Zhang, "Image compression with edge-based inpainting," IEEE Transactions on Circuits and Systems for Video Technology, vol.17, no.10, pp.1273–1287, 2007.

[27] Z. Xiong, X. Sun, and F. Wu, "Block-based image compression with parameter-assistant inpainting," IEEE Transactions on Image Processing, vol.19, no.6, pp.1651–1657, 2010.

[28] D. Liu, X. Sun, and F. Wu, "Inpainting with image patches for compression," Journal of Visual Communication and Image Representation, vol.23, no.1, pp.100–113, 2012.

[29] Z. Wang, A.C. Bovik, H.R. Sheikh, and E.P. Simoncelli, "Image quality assessment: From error visibility to structural similarity," IEEE Transactions on Image Processing, vol.13, no.4, pp.600–612, 2004.

[30] H.R. Sheikh, M.F. Sabir, and A.C. Bovik, "A statistical evaluation of recent full reference image quality assessment algorithms," IEEE Transactions on Image Processing, no.15, no.11, pp.3440–3451, 2006.

Akira Tanaka   received the D.E. degree from Hokkaido University, Sapporo, Japan, in 2000. He is with the Graduate School of Information Science and Technology, Hokkaido University. His research interests include image processing, acoustic signal processing, and machine learning.

Miki Haseyama   received her B.S., M.S. and Ph.D. degrees in Electronics from Hokkaido University, Japan in 1986, 1988 and 1993, respectively. She joined the Graduate School of Information Science and Technology, Hokkaido University as an associate professor in 1994. She was a visiting associate professor of Washington University, USA from 1995 to 1996. She is currently a professor in the Graduate School of Information Science and Technology, Hokkaido University. Her research interests include image and video processing and its development into semantic analysis. She has been a Vice-President of the Institute of Image Information and Television Engineers, Japan (ITE), an Editor-in-Chief of ITE Transactions on Media Technology and Applications, a Director, International Coordination and Publicity of The Institute of Electronics, Information and Communication Engineers (IEICE). She is a member of the IEEE, IEICE, ITE and ASJ.

Takahiro Ogawa   received his B.S., M.S. and Ph.D. degrees in Electronics and Information Engineering from Hokkaido University, Japan in 2003, 2005 and 2007, respectively. He joined Graduate School of Information Science and Technology, Hokkaido University in 2008. He is currently an associate professor in the Graduate School of Information Science and Technology, Hokkaido University. His research interests are multimedia signal processing and its applications. He has been an Associate Editor of ITE Transactions on Media Technology and Applications. He is a member of the IEEE, ACM, EURASIP, IEICE, and ITE.